

Towards a numerical modeling of the coupling between RTM process and induced mechanical properties for rigid particle-filled composites

Ahmed El Moumen

abdelghani saouab (✉ abdelghani.saouab@univ-lehavre.fr)

Universite le Havre: Universite du Havre

Abdellatif Imad

Toufik Kanit

Research Article

Keywords: Resin Transfer Molding, Particle-filled composite, Process/Properties coupling, Computational homogenization

Posted Date: September 9th, 2022

DOI: <https://doi.org/10.21203/rs.3.rs-2007582/v1>

License: © ⓘ This work is licensed under a Creative Commons Attribution 4.0 International License.

[Read Full License](#)

Towards a numerical modeling of the coupling between RTM process and induced mechanical properties for rigid particle-filled composites

Ahmed El Moumen (a), Abdelghani Saouab (a)*, Abdellatif Imad (b), Toufik Kanit (b)

(a) Normandie Univ, UNIHAVRE, CNRS, LOMC, 76600 Le Havre, France

(b) Unité de Mécanique de Lille, Université de Lille, Lille, France.

* abdelghani.saouab@univ-lehavre.fr

Abstract:

In this work, a method is proposed for modeling RTM process and the associated mechanical behavior of composites filled with mono-sized spherical Alumina particles. This method combines (i) a numerical model (RTM model) that allows the simulation of the RTM process during the injection of particle filled resins, and (ii) a computational strategy of mechanical properties based on the homogenization methods. These proposed models have already been validated with experimental results. The RTM model is based on 3 sub-models: the first one to describe the suspension flow, the second one to simulate the advance of the flow front, and the last one to model the particles filtration by the fibrous medium. The distribution result of the concentration of particles in the fibrous medium obtained at the end of the simulation of the injection is used as input data for mechanical models of homogenization. The homogenization numerical model was constructed from a representative volume element of the microstructures using the Poisson process. The idea here is to couple these two steps (RTM simulation + mechanical properties computation) in a complete model which allows at the same time and in a single operation: to simulate the process of the manufactured composites loaded with particles and to deduce their induced mechanical properties. The pertinence of the proposed method is confirmed by the simulation of nine elastic properties of composites with the finite element method. The influence of post-filling on the induced mechanical properties has been studied.

Keywords: Resin Transfer Molding, Particle-filled composite, Process/Properties coupling, Computational homogenization.

1. Introduction

Composite materials undergo continuous development in many industrial domains, especially in the transport sector. Compared to other conventional materials, composite materials have remarkable characteristics such as high specific strength, specific modulus and lightness. These many features can be extended by adding new specific functionalities to the composite materials by incorporating fillers (particles) into the material. These so-called functional composites can achieve a wide range of new properties, such as thermal [1] and electrical conductivity/insulation, magnetic or optical functionalities, and specific properties [2-3] such as fire resistance, abrasion resistance, electromagnetic shielding and self-healing [4-5]. Their advantages also include the improvement of existing properties, such as weight savings and amelioration of mechanical properties [6-7]. Tailored properties of composites are thus obtained by adding fillers to the composite material during fabrication [8]. These properties result from the physical characteristics of the particles, their volume ratio and their distribution in the composite.

The incorporation of particles into composite materials can be achieved by two methods [9-10], either by depositing inclusions on the surface of the preform (preform functionalization), or by adding particles to the liquid resin and injecting the suspension obtained into the fibrous medium (resin functionalization). In the last method, the liquid composite molding (LCM) processes, are common techniques used for the fabrication of particle loaded composites. For example, resin transfer molding (RTM) or vacuum assisted resin transfer molding (VARTM) was used with a suspension to achieve certain properties in the composite, such as electrical [11-12] and thermal conductivity [13-14] flame retardancy [15-18] self-healing properties [19], enhancement of mechanical properties [20-21] and weight-saving [22-24]. However, in LCM processes, the resin functionalization becomes more challenging as it affects the impregnation of the fibrous medium by the suspension and induces three main issues: an increase in the suspension viscosity, a filtration of particles by the fibrous medium and a non-homogeneous particle distribution within the finished part [25-28]. This crucial issue of the elaboration of functional composites by LCM processes comes from the complexity of particle addition to their fibrous structures. Indeed, the filtration of particles is a complex phenomenon that depends on several parameters related to the process and the different materials used. Therefore, the control of particle infiltration necessarily requires a good understanding of the physics of the

process and the influence of these parameters on the final properties of the structure. Numerical modeling of the process/properties coupling is an undeniable tool to help overcome this difficulty. Indeed, the desired properties result from the final distribution of the particles within the fibrous medium and this distribution is controlled by the process parameters involved.

Given the interest of the subject, and despite the complexity of studying suspension flow through fibrous media, a number of modeling efforts have been conducted; such as the work of Erdal et al [29], Lefevre et al [30], Qian et al [31], Abliz et al; [32] and da Costa [33], in which macroscopic models governing the filtration problems have been introduced to model the suspension flow in textile preforms. These models take into account the coupling between filtration and flow and allow the prediction of the evolution of the particle concentration during the impregnation of the fibrous medium. However, to our knowledge, apart from our study [1] dedicated to the coupling between RTM process and electrical properties of a particle-reinforced carbon-epoxy composite laminate, no numerical study on the process/properties coupling during the elaboration of particle-filled composites has yet been presented.

The objective of this paper is to develop a global modeling approach, which simulates both the fabrication of a particle-filled composite by RTM process and the prediction of its induced mechanical properties. The method proposed combines (i) a numerical model (RTM model) that allows the simulation of the RTM process during the injection of particle filled resins, and (ii) computational homogenization methods of the mechanical properties of composites using the out-put results of (i)-step. The RTM model [34-36] is proposed to describe the coupling between the suspension flow and the particle filtration by the fibrous medium during the RTM process. Then, the prediction of the mechanical properties is obtained by a computational homogenization method based on RVE and finite element method (FEM) as given in [37-40]. The idea here is to couple and assemble these two steps (RTM modeling + computational homogenization) in a complete model, to simulate the final distribution of particles in the fibrous medium at the process end, and to compute the induced mechanical properties of the composite, especially: Young's moduli E_{11} , E_{22} and E_{33} , shear moduli G_{12} , G_{13} and G_{23} , and Poisson ratio ν_{12} , ν_{13} and ν_{23} . In the following, a detailed presentation with various validations of the RTM model and the methods used for the homogenization of the mechanical properties is given. Then, different applications of the global modeling approach which couples the process simulation and the mechanical calculation are proposed.

2. The strategy of coupling RTM model / mechanical properties computation

During the RTM process, the injection of resins loaded with certain fillers such as Alumina particles, leads to an improvement of the mechanical properties of the manufactured composite. These induced properties are directly dependent on the final distribution of particle concentrations in the fibrous medium, which in turn is linked to the process parameters used. To describe this link between process and properties, we propose a coupling strategy between the RTM model and the computation of mechanical properties. This approach also shows how the process parameters can be used to control the mechanical properties of the composite. Figure 1 presents a description of the general principle of this strategy. This figure was divided into two parts: (i) the first part describing the RTM model (flow and filtration) coupled with a second part (ii) representing the computational of mechanical properties of composites. The coupling is formulated by introducing the simulation results of the process (i.e. the final concentration distribution of the particles in the fibrous medium) as input data for the second step of the mechanical properties homogenization.

In the study of process/property coupling, reducing the cost of computational time is an important issue. It is essential to optimize the proposed models to simulate the process and property computation.

In a previous work [26], we proposed an approach to model the RTM process with a particle filled fluid. This approach uses a stokes-Darcy coupling to describe the suspension flow at the mesoscopic scale and a "solid" model to model the mass dynamics of the particles and their retention, based on the equations of motion of each particle. Considering the large number of particles involved in the suspension during the injection, the use of this model in the framework of this work of coupling Process/Properties will generate rather long calculation times. For this reason, a modeling approach at the macroscopic scale much less greedy in calculation time will be used.

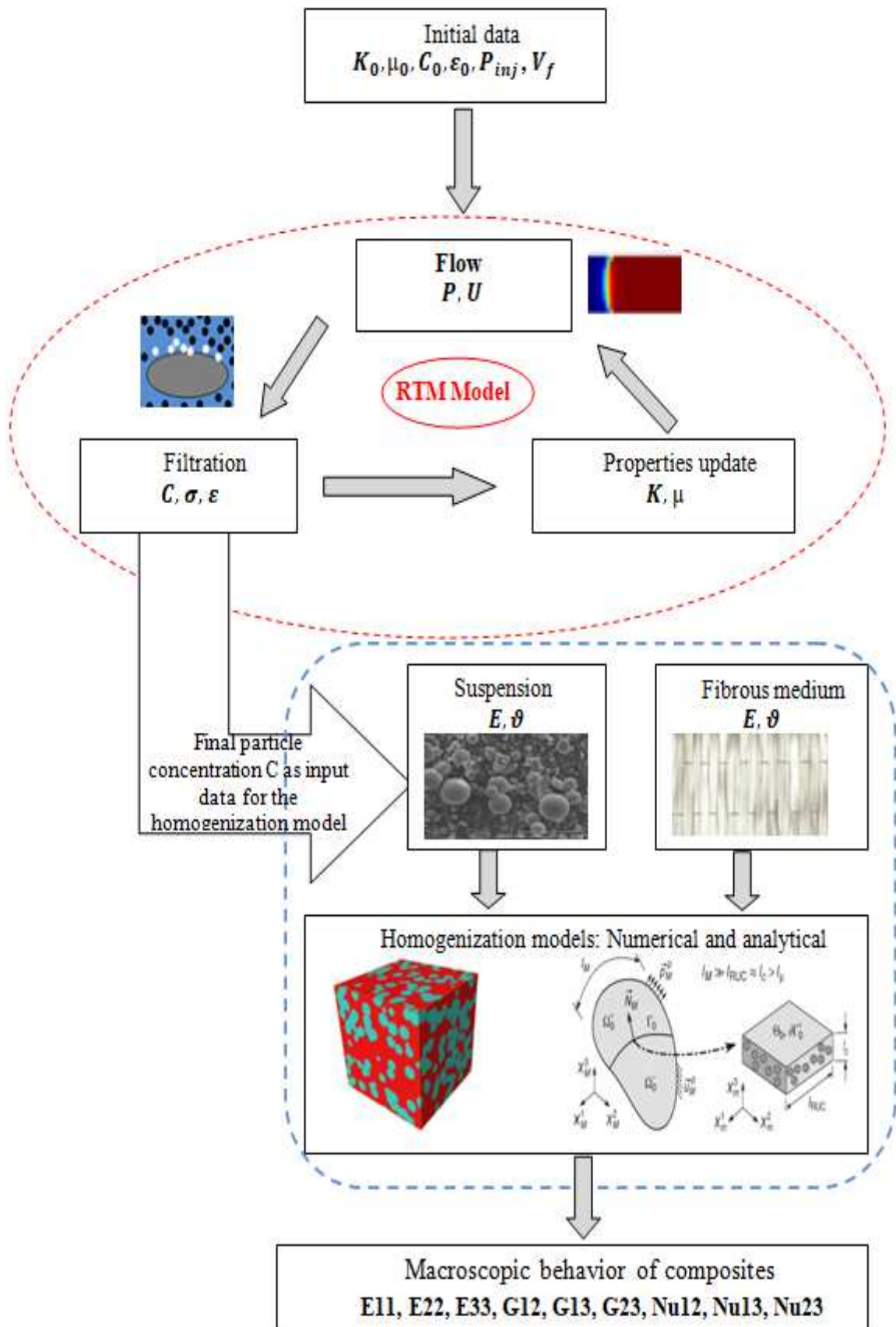


Figure 1: Illustration of the coupling strategy between the RTM model and the computation of mechanical properties.

3. Modeling of the RTM process

3.1. Governing Equations

On a macroscopic scale, the flow of a suspension (particles filled-resin) through a fibrous medium can be described using Darcy's law, as follows [1] [34]:

$$U = -\frac{K}{\mu} \nabla P \quad (1)$$

Where U, K, μ and P are the flow velocity, the permeability of the medium, the suspension viscosity and the pressure, respectively. The mass conservation equation can be expressed by the continuity equation given as:

$$\text{div} (U) = 0 \quad (2)$$

The combination of equations (1) and (2) leads to the governing equation of the pressure field which drives the flow:

$$\text{div} \left(\frac{K}{\mu} \nabla P \right) = 0 \quad (3)$$

The particles presence in the fluid causes an increase in the suspension viscosity and the suspension flow through the fibrous medium leads to particle filtration and consequently to a reduction in the porosity and the permeability of the fibrous medium. During the impregnation, two types of particles are distinguished: the trapped particles (or retained particles), with a volume fraction, noted σ hereafter, and the moving particles with a volume fraction noted εC , where ε is the porosity of the filter medium and C is the concentration of particles. The volume fractions of trapped and moving particles vary in the impregnated fibrous medium as a function of time and space. Retention σ and porosity ε of the fibrous medium can be related by the equation (4) [30]:

$$\varepsilon = \varepsilon_0 - \sigma \quad (4)$$

Where ε_0 is the initial filter porosity, corresponding to the fibrous medium porosity.

To model the dispersion of particles in the laminar flow through the fibrous media, an approach based on the calculation of the concentration of particles C is used. This approach is based on the advection transport equation, which results from the mass equation for the particles [10]. This model was expressed as follows:

$$\frac{\partial(\varepsilon C + \sigma)}{\partial t} + \nabla \cdot (UC) = 0 \quad (5)$$

Where the terms $\left(\frac{\partial(\epsilon C)}{\partial t}\right)$ represent the variation rate of the concentration of the moving particles, $(\nabla \cdot (\mathbf{UC}))$ the advection effect and $\left(\frac{\partial \sigma}{\partial t}\right)$ the deposit effect.

During the impregnation of a fibrous medium, the retention phenomenon is modeled by the following constitutive law [10]:

$$\frac{\partial(\sigma)}{\partial t} = UC\alpha\left(1 - \frac{\sigma}{\sigma_u}\right) \quad (6)$$

Where σ_u is the maximum possible deposit of particles that can be filtered by the fibrous medium, and α is the filtration coefficient variable as a function of the permeability K and the porosity ϵ . This equation describes the kinetics of the retention with a possible re-suspension of the particles. It relates the variation of the particles retained and filtered to the volume flow of the entering particles by the filtration coefficient α . In its second limb, the first term corresponds to the particle retention which is proportional to the flow of suspended particles UC and the second term represents the rate of re-suspension of the particles.

According to Erdal [29], the filtration coefficient α varies during the impregnation of the fibrous medium. It can be modeled as a function of permeability K and the porosity ϵ , as follows:

$$\alpha = \alpha_0 \left[\left(\frac{K}{K_0} \right)^{-1/2} \left(\frac{\epsilon}{\epsilon_0} \right)^{3/2} \left(\frac{1-\epsilon}{1-\epsilon_0} \right)^{-1} \right]^{a_1} \quad (7)$$

Where a_1 is the model constant and α_0 is the initial filtration coefficient.

The permeability evolution of the filter medium (fibrous medium + particles) can be modeled using the model presented in [28]. This relationship predicts the filter permeability as a function of the changing porosity as:

$$K = K_0 \left[\left(\frac{\epsilon}{\epsilon_0} \right) \left(\frac{1-\epsilon}{1-\epsilon_0} \right)^{-2} \right] \quad (8)$$

During the injection of the suspension, the porosity ϵ was affected by the local deposit particles via Eq. (4), which in turn affects the filter permeability via Eq. (8) and the filtration coefficient via Eq. (7). The spatio-temporal variation of the suspension viscosity is directly related to the concentration evolution of the particles. It can be predicted according to the relation (9) [28]:

$$\mu = \mu_0 \left(1 - \frac{C}{A}\right)^{-2} \quad (9)$$

Where μ_0 is the viscosity of the neat resin and A is an empirical constant obtained via experimental data.

3.2. Flow front advancement

During impregnation, the fibrous medium saturation by the suspension can be described by a function ϕ (Level set function). We can distinguish two zones: a completely saturated region where $\phi = 1$ and a dry region where $\phi = 0$. The interface between these two sub-domains is defined by $0 < \phi < 1$. The computational domain corresponds to the region of the fibrous medium saturated with the suspension. It has a mobile border, which varies during the impregnation: the flow front. To determine its position during the injection, the level set method is used [13]. The principle of this method consists in determining a “level set function” ϕ by solving the transport equation (10) based on the advection of this function by the flow velocity and the interface thickness:

$$\frac{\partial \phi}{\partial t} + U \nabla \phi = \gamma \nabla (v \nabla \phi - \phi(1 - \phi) \frac{\nabla \phi}{|\nabla \phi|}) \quad (10)$$

Where γ is the reinitialization parameter used to control the instability of the flow and v the adjustable thickness of the interface. The position of the flow front is determined by tracking the “level set function” with a value of 0.5 (see Figure 2).

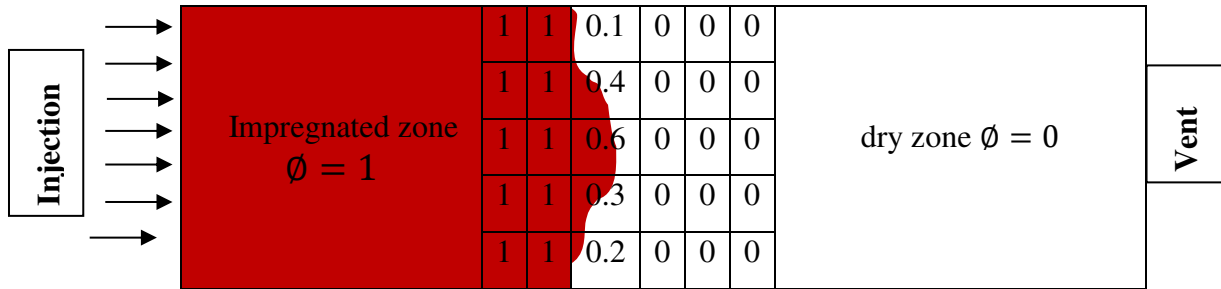


Figure 2: Illustration of the level set function variation during RTM process.

3.3. RTM numerical computation

The presented model is used to simulate the injection of suspension in the RTM process. At the initial time $t=0$, we impose at any point x of the fibrous medium, the particles concentration $C(x, 0) = 0$, the retention $\sigma(x, 0) = 0$, the pressure $P(x, 0) = 0$ and the porosity $\varepsilon(x, 0) = \varepsilon_0$.

As boundary conditions, we imposed at the inlet ($x = x_0$) during the injection: $C(x_0, t) = C_i$, $Q(x_0, t) = Q_{inj}(t)$ or $P(x_0, t) = P_{inj}(t)$ and at the vent ($x = x_e$): $P(x_e, t) = 0$. For the wall boundary, we applied a Dirichlet condition (impermeable wall). C_i is the concentration of initial fillers in the suspension, P_{inj} is the injection pressure and Q_{inj} is the injection flow rate.

The various equations of the model were implemented in the commercial software COMSOL Multiphysics 5.4, via the partial differential equations (PDE's) package. The equation system composed of Darcy's law (1), governing equation of the pressure field (3), the continuity equation for particles (5), and the filtration kinetic equation (6), is solved in order to determine the flow unknowns: pressure P , velocity U , particle concentration C and the retention σ .

3.4. Validation of the RTM numerical model

The numerical model proposed in this study was validated by a comparison with experimental results and the analytical model, during a linear injection, which induces a unidirectional flow of the suspension through the fibrous medium. In the experimental case, the injection is carried out at imposed pressure and in the analytical case; the injection is conducted at imposed velocity. In the last case, if V_0 denotes the injection velocity of the used suspension, the front velocity is can be determined by:

$$U_f = \frac{V_0}{\varepsilon_0} \quad (11)$$

Indeed; at the flow front the retention can be considered null [28], therefore; according to equation (4), the front porosity is equal to the initial porosity ε_0 of the medium. Since ε_0 is constant, the integration of the equation (11) makes it possible to determine the front position X_f as a function of time:

$$X_f = \frac{V_0}{\varepsilon_0} t \quad (12)$$

The used velocities for analytical modeling are $V_1=0.85$ mm/s, $V_2=2V_1$ and $V_3=3V_1$. Table 1 presents the properties of the materials used and the conditions of the two tests considered in the experiment. In the first test, the suspension is constituted of epoxy resin and spherical boehmite nano-particles with an average diameter of 104 μm and the reinforcement is a quasi-unidirectional carbon- fiber textile. The injection experiments are carried out on a permeability test rig, which allows the extraction of fluid samples during impregnation and the observation of flow fronts. The injections are conducted at constant pressure of up to 3 bar. The

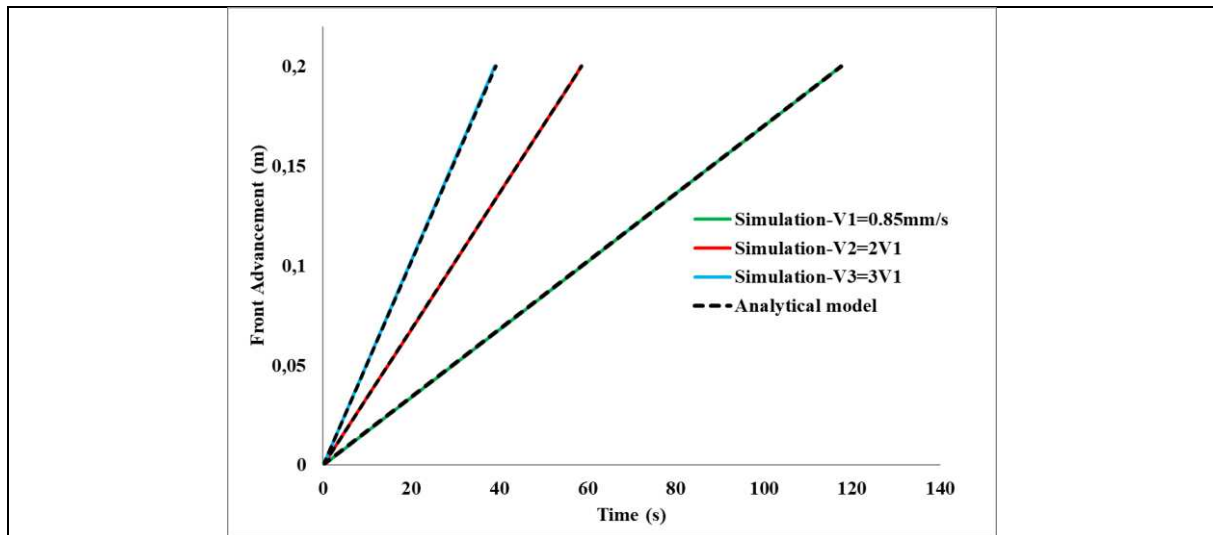
injected suspension is extracted at five locations between the inlet and the outlet every 5 cm. Then, the concentration of particles in the extracted samples is measured by thermo-gravimetric analysis on a TA Instrument TGA Q5000. In the second test, the suspension is prepared based on polyester resin and spherical micro-beads having a diameter of 12 μm and synthetic PET fibers felt is used as reinforcement. The experimental setup is composed of a rigid tooling (steel half mold and thick PMMA top plate). The mold is fed at constant pressure using a pressure bucket, equipped with a motorized mixer so as to maintain a homogeneous blend of the suspension. The flow is monitored through the PMMA mold top plate that allows observations and to record the front kinetics. After polymerization, samples are cut out from the composite part at known locations. Samples are weighed, measured and burnt at high temperature (500 $^{\circ}\text{C}$) so that filler content can be evaluated at any distance from the inlet.

Parameters	Test 1 [32]	Test 2 [30]
C_i : Initial fillers concentration (% <i>vol</i>)	5.0	40.5
μ_0 : Viscosity of neat resin (Pa. s)	0.04	0.20
K_0 : Fiber permeability ($\ast 10^{-10}$) (m^2)	0.85	4.92
V_f : Fiber volume fraction (%)	50.0	18.7
α : Filtration coefficient (m^{-1})	0.2703	0.27
a_1 : Model constant	1.0	1.0
P_{inj} : Injection pressure (Pa)	1.10^5	2.10^5

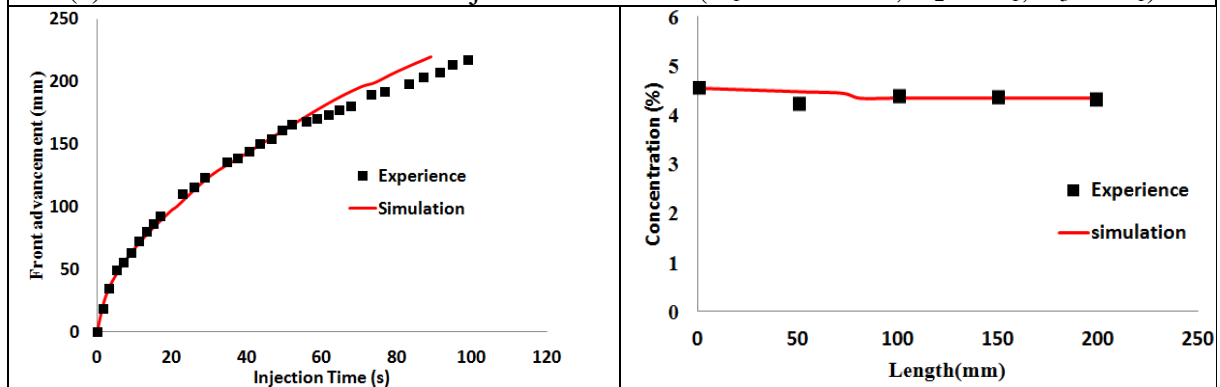
Table 1: Parameters used in the simulation.

Figure 3 presents the comparison of the numerical results of the proposed model with the experimental and analytical results. Figure 3 (a) describes the numerical and analytical kinetics of the flow front in the case of the injection velocities V_1 , V_2 and V_3 , while Figure 3 (b) and Figure 3 (c) describe the front kinetic and the final distribution of the particle concentration along the preform, respectively in the case of test 1 and test 2.

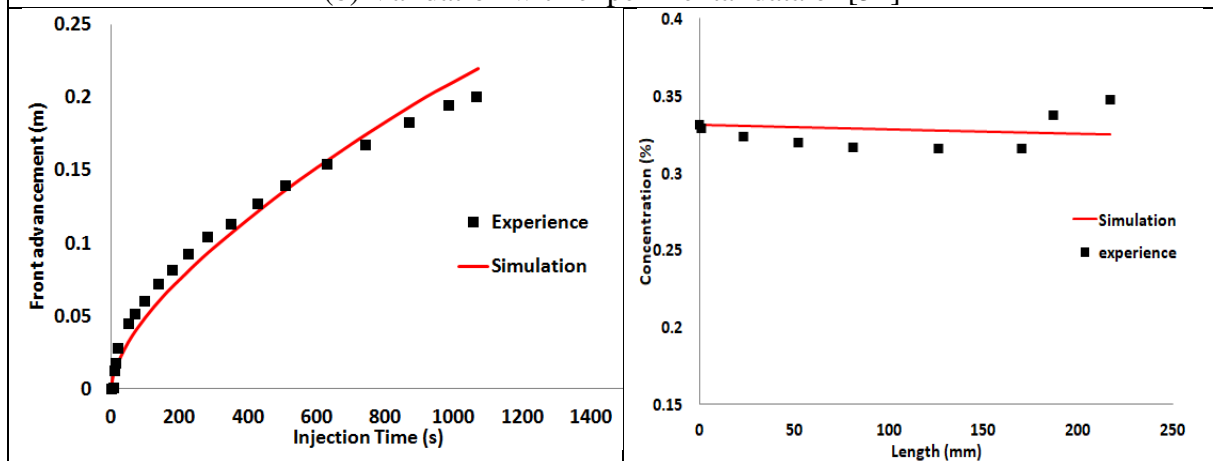
This comparison shows that the numerical results of the model are in good agreement with the analytical and experimental results. These results show very similar trends and profiles, especially in the analytical case, and a low relative error occurs in the experimental case: 4% (test 1, front advancement), 2% (test 1, concentration prediction), 6 % (test 2, front advancement), and 5% (test 2, concentration prediction).



(a) Front kinetic for different injection velocities ($V_1=0.85$ mm/s, $V_2=2 V_1$, $V_3= 3V_1$)



(b) Validation with experimental data of [32]



(c) Validation with experimental data of [30]

Figure 3: Comparison and validation of the numerical model with: (a) analytical and (b, c) experimental results.

3.5. Numerical results of RTM model

In this section, the numerical results of the RTM process simulation were presented and discussed. For that, a linear injection of a suspension (resin epoxy + particles), through a preform (UD glass fibers) of rectangular geometry, at imposed injection velocity V_i was

considered. The injection threshold is placed on the entire left edge of the preform and the vent is placed on the right one (see Figure 2). The preform has a rectangular geometry of length $L = 0.2$ m and height $h = 0.01$ m. The features of materials, parameters of the numerical model and injection conditions considered are detailed in Table 2.

μ_0 : Viscosity of neat resin (Pa. s)	0.1	α_0 : Initial filtration coefficient (1/m)	1
K_0 : Fiber permeability (m^2)	2.10^{-10}	σ_u : Ultimate specific deposit	0.5
V_f : Volume fraction of fiber (%)	50	a_1 : Parameter model	1
V_i : Injection velocity (mm/s)	1.7	C_i : Initial fillers concentration (%vol).	20

Table 2: Physical properties of materials and parameters used for the numerical simulation.

The injection of the suspension was controlled at different times. Figure 4 shows the filling state at different times (10s, 20s, 30s and 58s). The fibrous medium saturation is described by the level set function ϕ . The completely saturated region where $\phi = 1$ is represented by the red color, and the dry region where $\phi = 0$ is in blue. This figure shows also an enlargement at the interface level between these two sub-domains where $0 < \phi < 1$. It reveals the capacity of the Level set method to describe this fine interface.

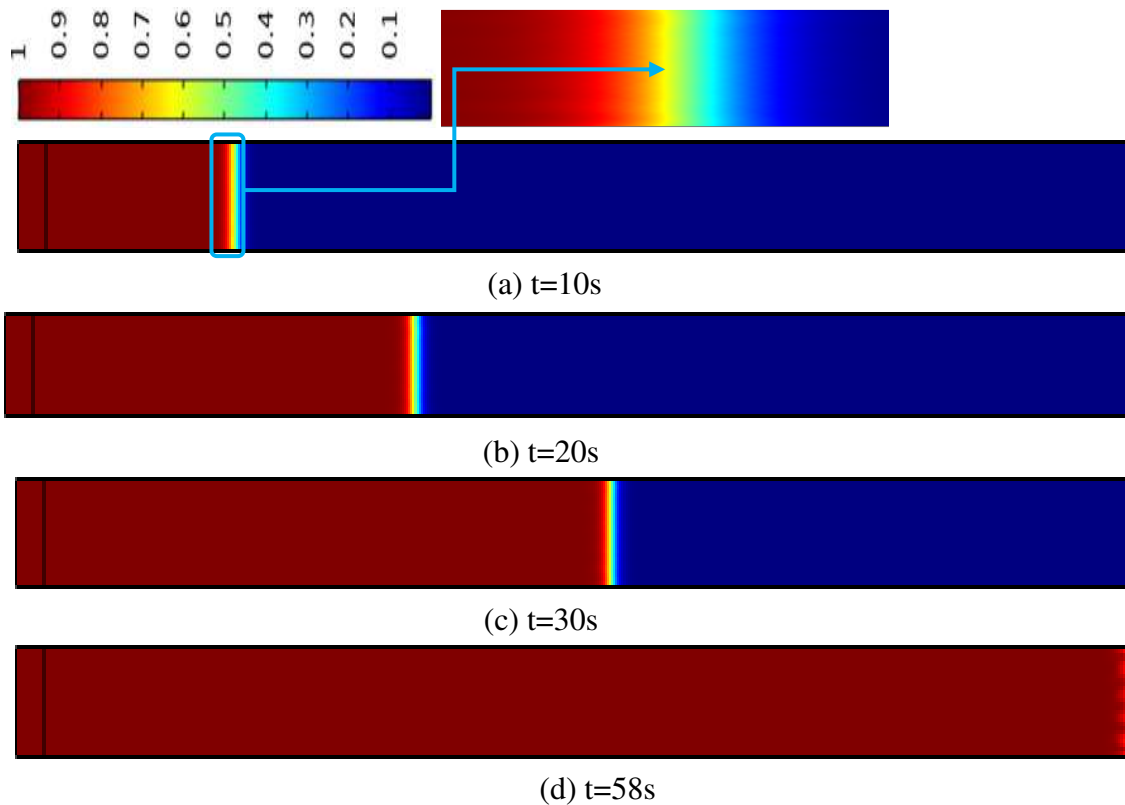
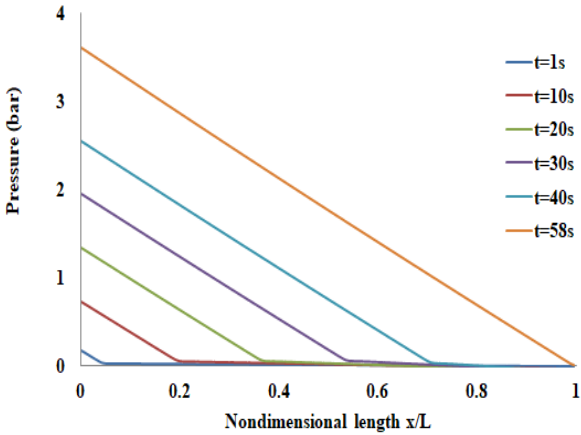
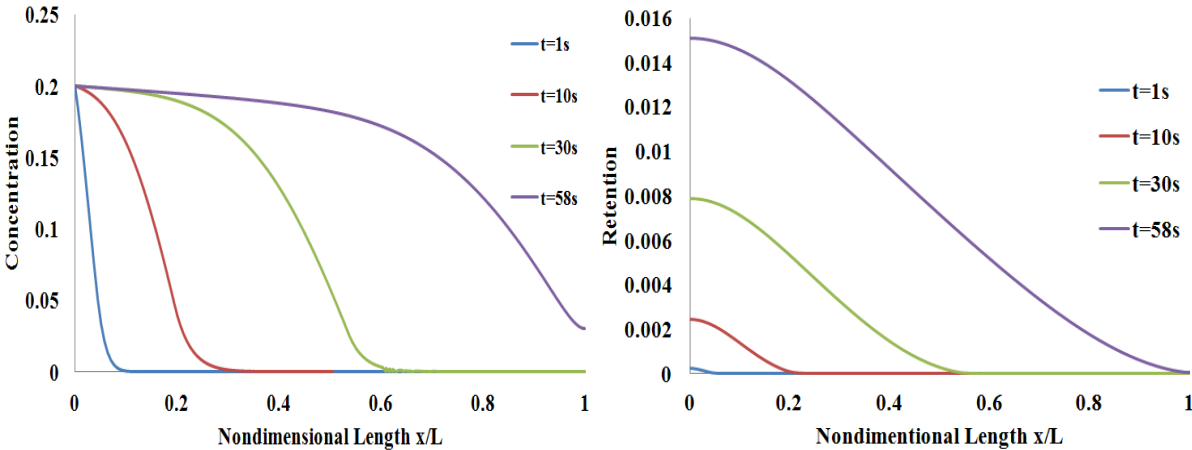


Figure 4: Fibrous medium saturation during suspension injection for different times: (a) $t=10s$, (b) $t=20s$, (c) $t=30s$, (d) $t=58s$.

The kinetics of the flow front obtained during this simulation is discussed. As expected, a linear profile is obtained and it is noted that the complete filling of the mold is reached after 58.5s. Figure 5 describes the evolution of the pressure field, the concentration and the retention of the particles during the impregnation.



(a) Pressure evolution



(b) Concentration and retention evolution

Figure 5: Evolution of the pressure, concentration and retention during injection:(a) Pressure evolution and (b) concentration and retention evolution.

It is noted that the pressure curves (Figure 5 a) have a decreasing linear profile and the slopes which increase continuously during the injection. This is due to the increase in the pressure at the injection threshold, which from the value 0.1 bar at $t=1s$, reaches 3.6 bar at the end of the injection. Figure 5b shows the curves of particle distribution and retention in the saturated area of the preform, during the injection. These curves have a descending profile and show a non-homogeneous distribution of moving or captured particles. At the end of the impregnation, a high particle concentration, greater than 15%, was distributed along $\frac{3}{4}$ of the preform length, followed by a sudden and high decrease in the distribution of the particles on

the rest of the preform. While a small quantity of particles is retained by the fibrous medium and accumulates in the vicinity of the injection threshold ($\sigma = 1.5\%$).

Figure 6 shows the spatial variation of the viscosity, permeability and particle concentration at the end of the impregnation. The concentration and the viscosity present a similar decreasing profile and the permeability a rather increasing profile. These curves reflect the influence of the particles on the modification of the behavior of the viscosity and the permeability and therefore on the flow.

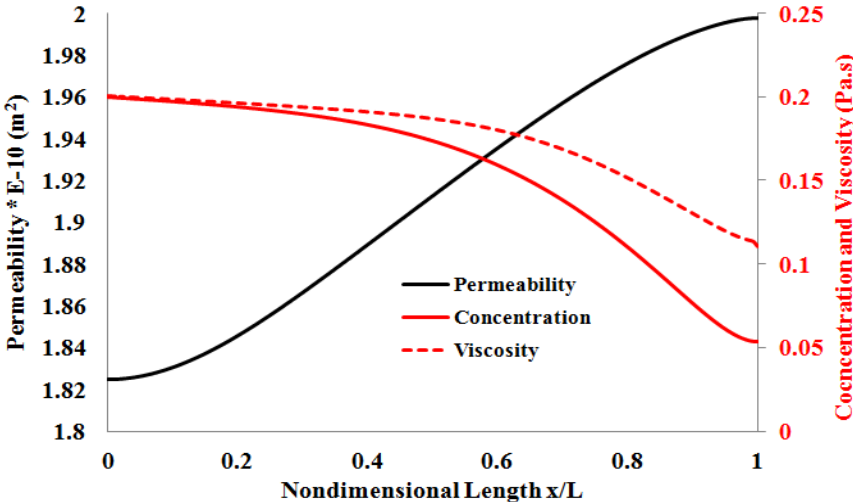


Figure 6: Concentration, viscosity and permeability profiles at the end of the impregnation (at time $T_f=58s$)

From the results of the simulation, it appears that the distribution of particles is non-uniform through the medium when the mold was completely filled at $t=58s$. To improve the distribution of particles, the impregnation will be continued after the mold filling and the suspension was evacuated from the outside of the mold through its vent. Figure 7 shows the effect of the injection time on the distribution of the particles. From this figure, it appears that a clear amelioration is obtained in the particle distribution at $t=70s$, and a quasi-constant profile was obtained for 80, 90 and 100s. The final concentration at the vent was 17.22% for $t=90s$ instead of 4.26% at $t=58s$. Figure 8 illustrates this amelioration for different injection times.

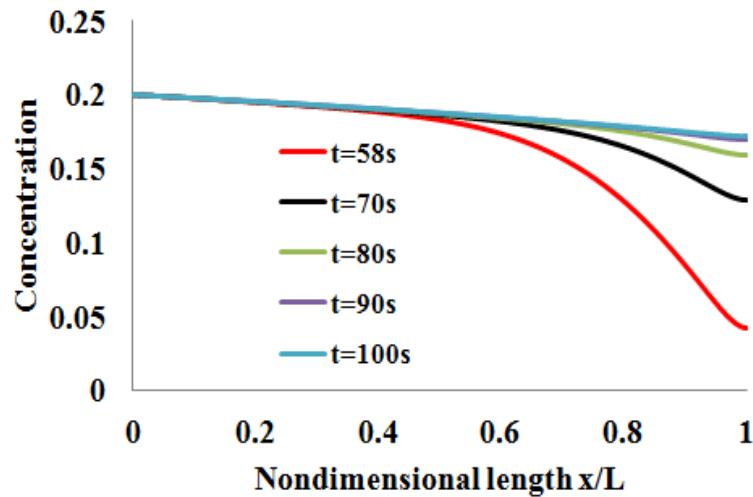


Figure 7: Evolution of the concentration after the total mold filling.

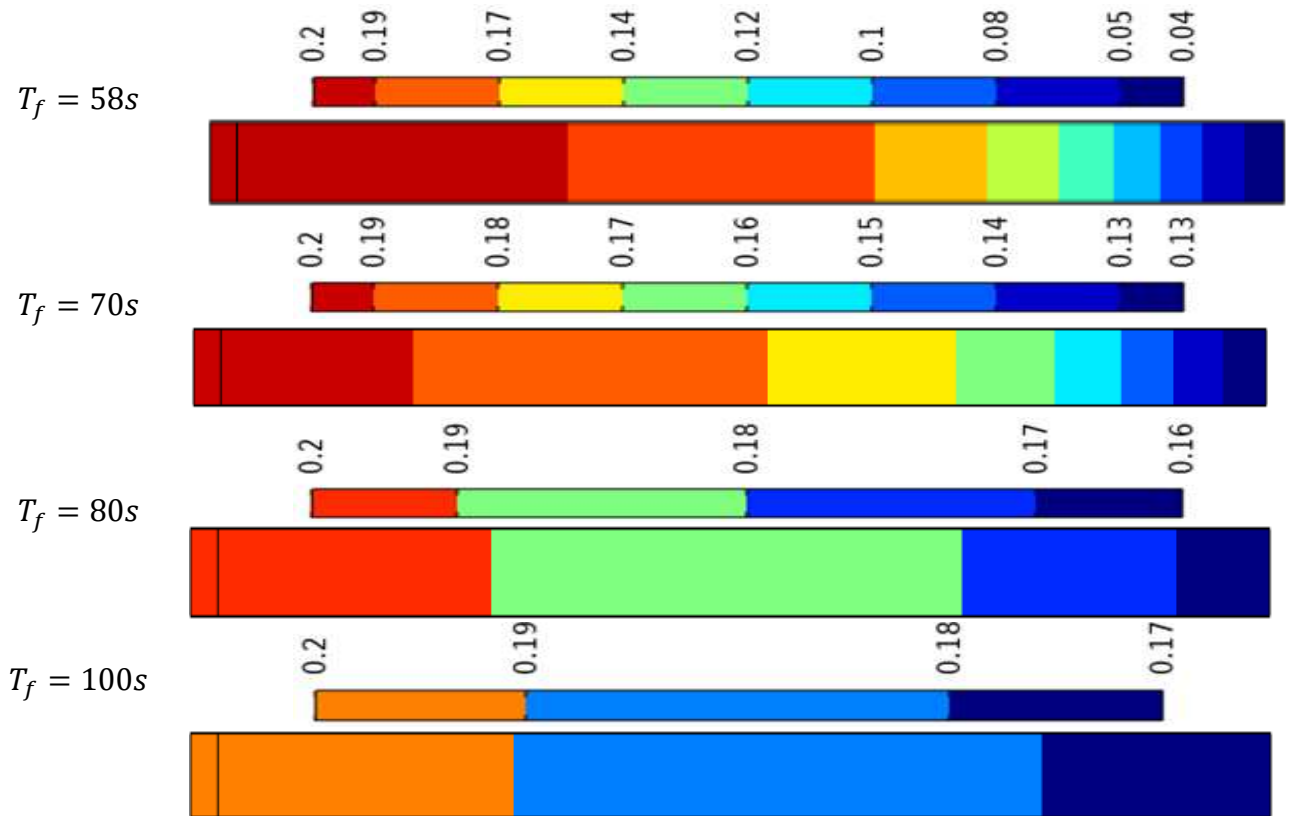


Figure 8: Evolution of the concentration for different injection times.

4. Computational homogenization of the mechanical properties

4.1. Description of the homogenization method

The multi-scale architecture of the studied composites is more complex. It consists of three different phases: resin, mono-sized spheres and the unidirectional (UD) fibers. Actually, there is no FE code can directly model such three phase's architecture. The proposed method

in this section consists of using two-step homogenization methods. This method is depicted in Figure 9.

Firstly, the mechanical behavior of the suspension (resin + mono-sized particles) is homogenized as a separate composite phase (composite 1), and then the obtained results are used as input data of the second step homogenization of composite 2 (composite 1 + UD fibers). The first step of homogenization was performed with the help of the numerical and the analytical models validated with experimental data and the second step of the homogenization was performed with the analytical models.

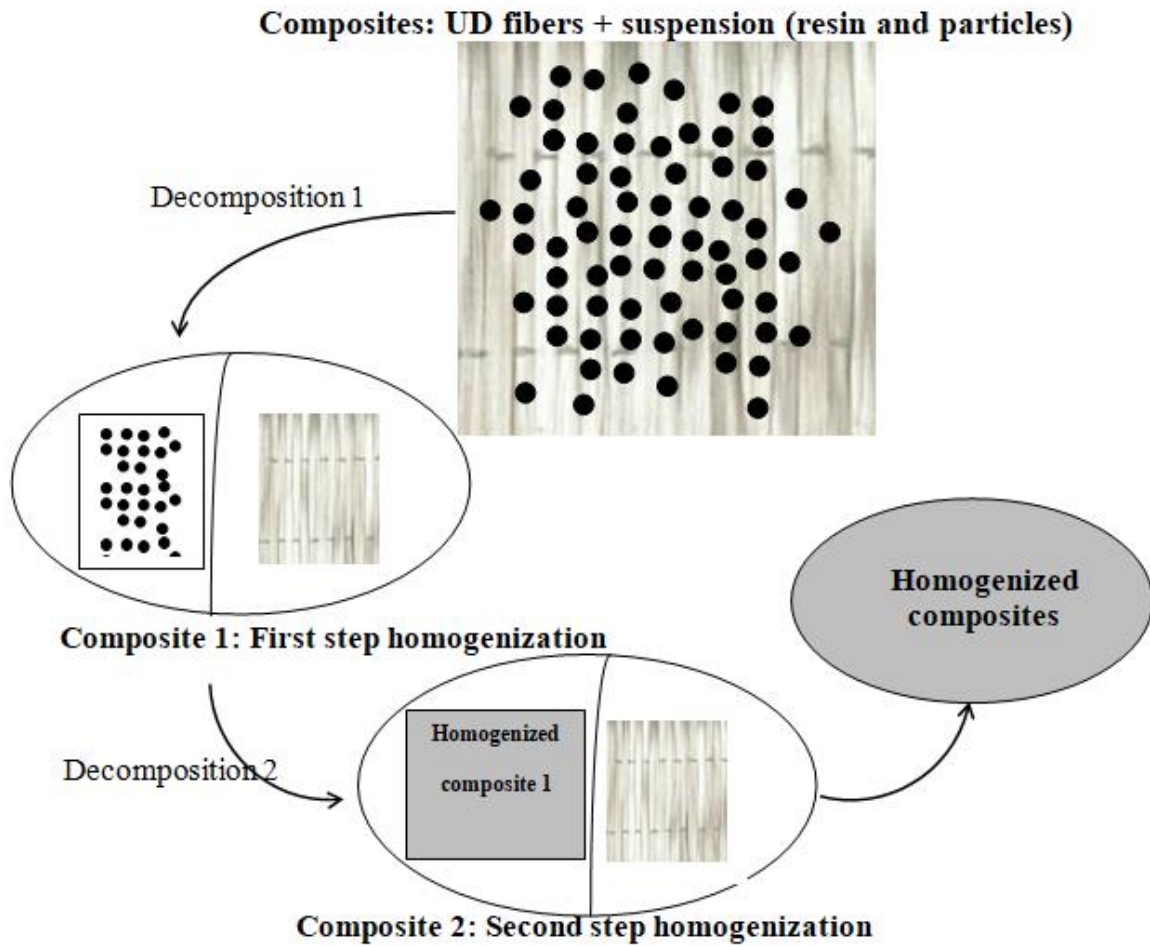


Figure 9: Two step homogenization method used in this study.

Suppose that the composite (suspension + UD fibers) is subjected to a macroscopic stress Σ and a macroscopic strain E . The objective of the homogenization is to determine the effective stiffness tensor \bar{C} of the composite and the effective compliance tensor \bar{S} such that:

$$\Sigma = \bar{C}:E \quad \text{and} \quad E = \bar{S}:\Sigma \quad (13)$$

For these tensors, the macroscopic fields are related to the averaged value of the local microscopic fields via the following equations:

$$\sigma(\mathbf{x}) = \mathbf{B}(\mathbf{x}) : \Sigma \quad \text{and} \quad \varepsilon(\mathbf{x}) = \mathbf{A}(\mathbf{x}) : \mathbf{E} \quad (14)$$

Where $\sigma(\mathbf{x})$ and $\varepsilon(\mathbf{x})$ are the local stress and strain fields and $\mathbf{A}(\mathbf{x})$ and $\mathbf{B}(\mathbf{x})$ are the strain and the stress localization tensor. The macroscopic fields are related to the local microscopic fields as:

$$\Sigma = \langle \sigma(\mathbf{x}) \rangle \quad \text{and} \quad \mathbf{E} = \langle \varepsilon(\mathbf{x}) \rangle \quad (15)$$

For the case of two-phase composite (resin and particles), the localization tensors of composites (A and B) are obtained as:

$$\langle \mathbf{A}(\mathbf{x}) \rangle = C_1 \mathbf{A}_1 + C_2 \mathbf{A}_2 \quad \text{and} \quad \langle \mathbf{B}(\mathbf{x}) \rangle = C_1 \mathbf{B}_1 + C_2 \mathbf{B}_2 \quad (16)$$

Where “j=1,2” denote the matrix and particles phase and C_j the concentration rate of phases.

4.2. Generation of RVE composite 1

The first step of the homogenization method consists of identifying and generating the numerical representative volume element (RVE) of the suspension. In principle, at each concentration of the particles in the composite, a VER will be associated. This RVE will then be discretized into cubic volume.

The technique used for generating the RVE for numerical homogenization computations is described in this section. Generally, the random sequential adsorption (RSA) algorithm [41] is the most used algorithm for generating random packing's. An improved version of the RSA algorithm was proposed in [42]. In this study, we will instead use the Poisson process. The associated algorithm was proposed in detail in our previous works [43-44], and it can be used for particles with ellipsoidal or cylindrical shapes.

At the beginning of the computation in this algorithm, the position of the first particle in the suspension is randomly selected. Then, the position of the second particle is drawn and the repulsion distance is checked between two neighboring particles. If there is overlapping between the particles' positions, the position of the second particle is drawn again until the repulsion distance was respected. This process is repeated until the desired volume fraction of particles. Table 4 present the used algorithm.

The particles are characterized by an orientation distribution function (ODF) that provides the probability of a particle to be oriented along with the defined tensor. In a global

coordinate system OXYZ, the particle orientation is defined by its two Euler angles, θ and β (Figure 10). For the particles, each one is characterized by its own unit orientation vector q , defined by θ and β as:

$$\begin{aligned} q_1 &= \cos\theta \\ q_2 &= \sin\theta\sin\beta \\ q_3 &= \sin\theta\cos\beta \end{aligned} \quad (17)$$

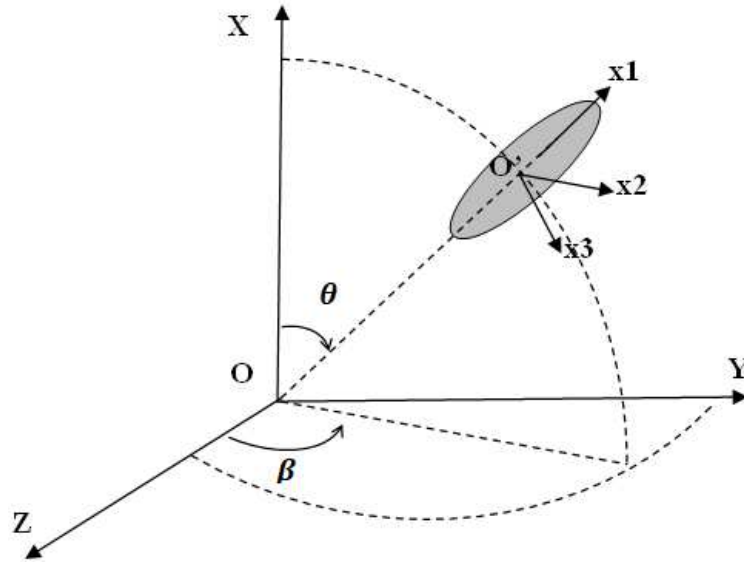


Figure 10: Two Euler angles $\theta \in [0, \pi]$ and $\beta \in [0, 2\pi]$ of particles with respect to the global Cartesian coordinate system (O, X, Y, Z) and the local Cartesian coordinate system (O', x1, x2, x3).

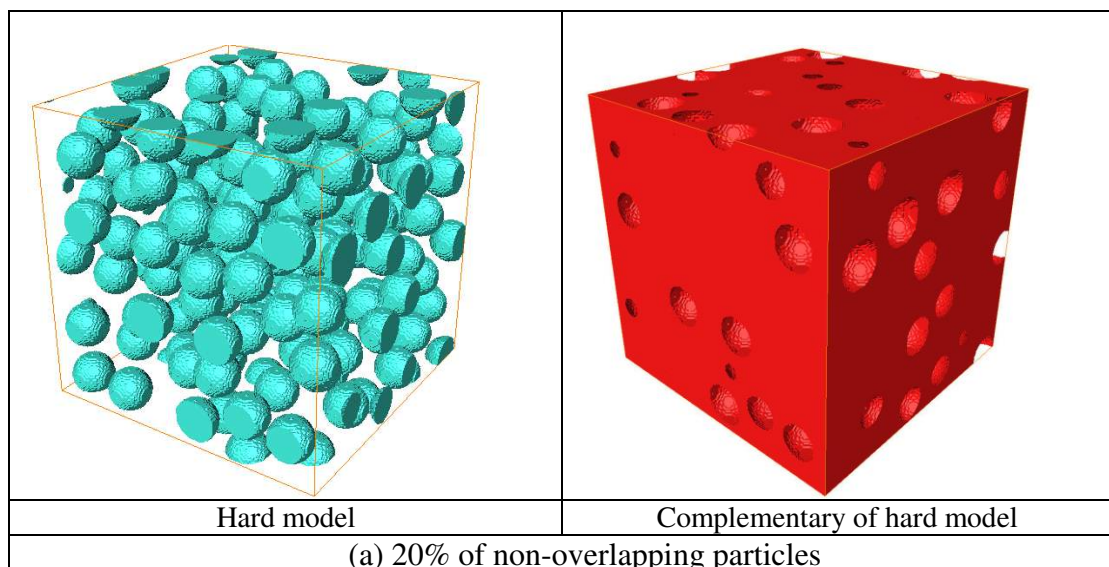
Main Algorithm
Input data: N, R1, R2, C ₀
Output: (a, b, c), r and q of all particles
1: define a RVE matrix with dimension LxLxL. Set a corner as the origin Set one of the matrix corners as the origin
2: for i=1 → N do
For each generated particles I
3: Assign a random position vector r_0^i
4: Assign a random quaternion vector q_0^i
5: end for
6: initialize the actual volume fraction C(t=0) = 0.
7: while C(t=0) < C ₀ do
8: Verify tc: Collision time between two ellipsoids
9: Verify ts: Collision time between particles and the cube faces
10: Compute $\Delta t = \min(tc, ts)$
11: for i=1 → N do
12: change de position: move the particle i from t to (t+Δt)
13: end for
14: if Δt ≤ tc then
15: update the position and the vector
16: else if Δt = ts then

17: create a periodic image of the concerned particle
18: end if
19: Compute the new volume fraction of particles: $C(\mathbf{t}+\Delta\mathbf{t}) = \frac{1}{L^3} \sum_{i=1}^N \frac{4}{3} \pi (\mathbf{a}_{\mathbf{t}+\Delta\mathbf{t}}^i \mathbf{b}_{\mathbf{t}+\Delta\mathbf{t}}^i \mathbf{c}_{\mathbf{t}+\Delta\mathbf{t}}^i)$
20: end while
21: continue the computations by adding the particles and changing the position until $C_{(\mathbf{t}+\Delta\mathbf{t})} = C_0$
N: Number of particles, Ri: radius of particles, (a, b, c) output dimension data of particles,

Table 4: Pseudo-code for generating particles in the suspension.

Figure 11 shows an example of random microstructures, generated using the Poisson process, containing 200 spherical particles (radius $R=100 \mu\text{m}$) with a particle volume fraction C_0 of 20%. The hard model, presented in Figure 11a, was generated with a repulsion distance $> 2R$, and the Boolean model of Figure 11b was generated with the possibility of particles overlapping. This last microstructure was considered in the calculations of the mechanical properties of the suspension (resin + mono-sized particles) to model the agglomeration phase. The complementary model of the hard and Boolean models, presented in Figure 11, corresponds to the resin part in the VER.

The microstructure of the suspension was analyzed with the help of SEM microscopy. Figure 12 shows the microscopic morphology of the suspension observed with SEM. Qualitatively, this morphology illustrates that the microstructure contains three scales: the scale of the resin, the scale of the aggregates and the scale of the particles. Looking at the microstructure of Figures 12b and 12c, generated with the Poisson process, it seems that the morphology contains the three scales as observed by SEM. A zoom-out in the aggregate phase, obtained by overlapping particles, is presented in Figure 12c. The contact between particles and the matrix was considered perfect without inter-phase.



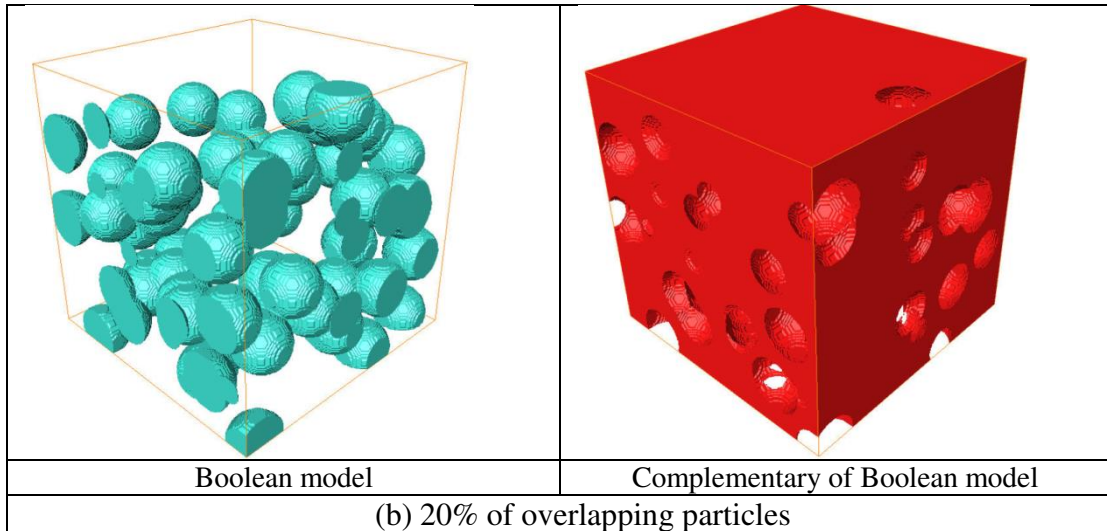


Figure 11: Generated microstructures for the simulation of the suspension behavior.

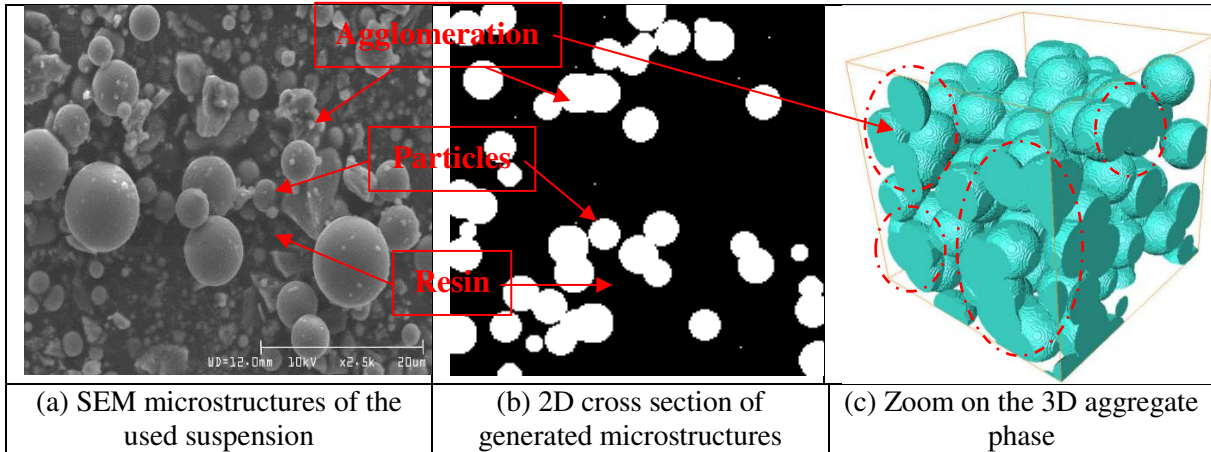


Figure 12: Comparison of the microstructures of SEM and those of Poisson process. 2D section showing three scales (matrix, particles and aggregates) and the zoom on the aggregates.

4.3. Meshing and the validation of models

Several techniques and software are available to mesh the RVE of microstructures. In this study, priority has been given to create a mesh that follows the constituents: particles, aggregates and the matrix. Digimat software was used to mesh the RVE of composite1 (suspension) with 300000 tetrahedral elements respecting the internal coarsening and curvature control of aggregates. The mesh density was determined for different mechanical properties. The chodral deviation ratio was also used to define the curved edge. Figure 13 presents an example of composite1 meshes.

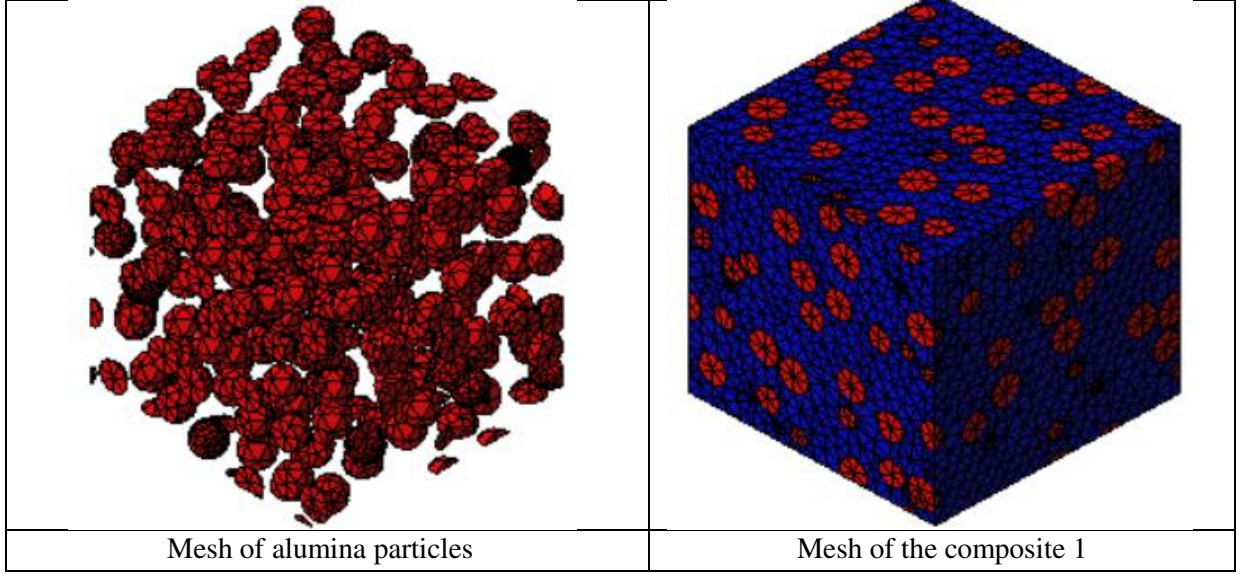


Figure 13: Example of meshes used in the simulation model.

For the computation of mechanical properties of composites, various analytical models can be found in the literature. A list of these models adapted for the used suspension reinforced with particles was presented by Al Habis et al. [45]. The popular existing approaches are: Mori and Tanaka model [46] (MT), Hashin and Shtrikman bounds [47] (HS) and the generalized self-consistent model [48] (GSC). These models allow to estimate the elastic properties of the suspension.

The mathematical expressions for HS bounds are given as:

$$k^{HS-} = k_m + \frac{p}{\frac{1}{k_i - k_m} + \frac{3(1-p)}{3k_m + 4G_m}}, \quad \text{and} \quad k^{HS+} = k_i + \frac{1-p}{\frac{1}{k_m - k_i} + \frac{3p}{3k_i + 4G_i}} \quad (18)$$

$$G^{HS-} = G_m + \frac{p}{\frac{1}{G_i - G_m} + \frac{6(1-p)(k_m + 2G_m)}{5G_m(3k_m + 4G_m)}}, \quad \text{and} \quad (19)$$

$$G^{HS+} = G_i + \frac{1-p}{\frac{1}{G_m - G_i} + \frac{6p(k_i + 2G_i)}{5G_i(3k_i + 4G_i)}}$$

Where k_i, G_i, k_m and G_m are the bulk and shear moduli for the particles i and matrix m respectively and p the concentration of particles. The symbols $+$ and $-$ indicates the upper and lower bounds of Hashin.

The expression of the MT model is given as:

$$k^{MT} = k_m \left(1 + \frac{p(k_i - k_m)}{k_m + a(1-p)(k_i - k_m)} \right), \text{ where } a = \frac{3k_m}{3k_m + 4G_m} \quad (20)$$

$$G^{MT} = G_m \left(1 + \frac{p(G_i - G_m)}{G_m + b(1-p)(G_i - G_m)} \right), \text{ where } b = \frac{6(k_m + 2G_m)}{5(3k_m + 4G_m)}$$

For the case of GCS, the expressions were proposed for shear and bulk moduli of the suspension. For the suspension shear modulus, the estimated property is the solution of this equation:

$$A \left(\frac{G^{GSC}}{G_m} \right)^2 + B \frac{G^{GSC}}{G_m} + C = 0 \quad (21)$$

Where the expressions of the coefficients A, B and C are specified in appendix A.

For the bulk modulus, the expression is:

$$k^{GSC} = k_m + \frac{p(k_i - k_m)}{1 + (1-p) \frac{k_i - k_m}{k_m + \frac{4}{3}G_m}} \quad (22)$$

The Young's modulus of the suspension was computed using this equation:

$$E = \frac{9k}{3k + G} \quad (23)$$

For the numerical model case, the simulation of a simple uni-axial test applied on the suspension RVE is used to compute the Young's modulus. The numerical results obtained are presented in Table 4 and compared with experimental data and analytical results. From these results, it appears that the experimental data and the numerical results are systematically between the HS bounds (HS+ and HS-) and close to the MT model. The numerical model and the analytical approaches were validated with the experimental data of [49].

	HS-	MT	Numerical	GSC	Experimental [49]	HS+
Young's modulus (GPa)	1.412	1.9106	1.88	1.9368	2.48 ± 0.5	12.52

Table 4: Comparison of different results: numerical and analytical results vs experimental data [49] of suspension with 20% of alumina particles.

Table 4 gives a comparison between mechanical properties obtained with different analytical, experimental and numerical results for a suspension reinforced with a random distribution of

alumina particles. The detail of the experiment part and the mechanical properties of each constituent were presented in [49].

Another comparison of the numerical and analytical models with experimental results of [40] is presented in Figure 14. This comparison clearly shows the good agreement between our numerical results compared with the experimental data and analytical models of MT and GSC. It can also be seen that the MT analytical model leads to results very close to the numerical and experimental results. Therefore, this analytical model MT was used, in order to reduce the computational time costs, to estimate the macroscopic mechanical properties of the suspension reinforced with spherical alumina particles.

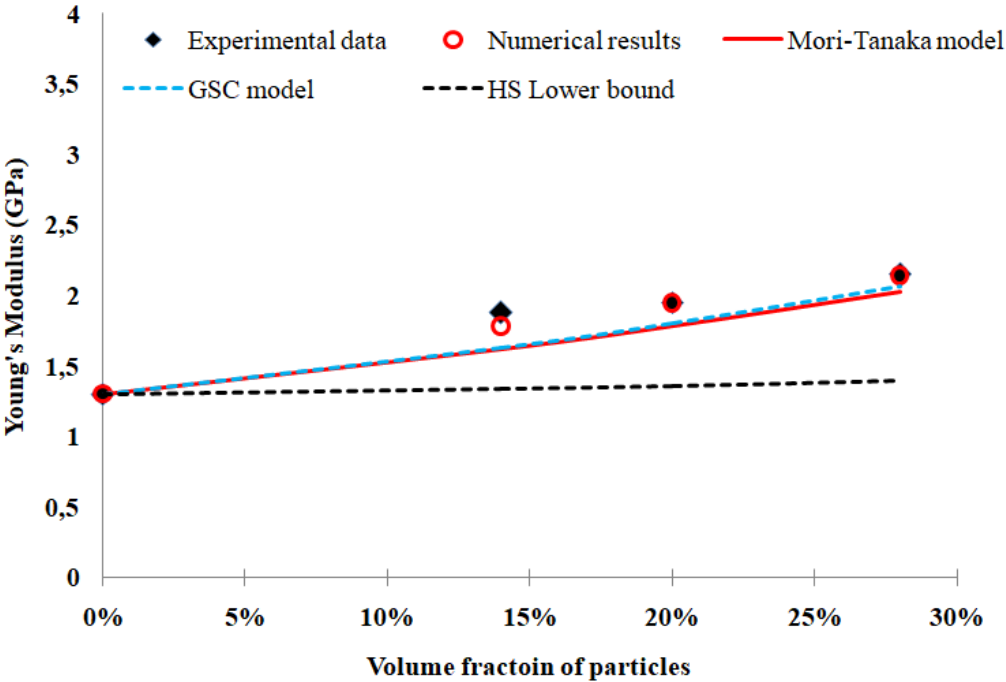


Figure 14: Comparison of numerical and analytical results with experimental data of [40].

Introducing the particles into suspension generates the agglomeration of particles and the concentration of stress when strength was applied. Figure 15 shows the distribution of the stress in the suspension under tensile and shear tests. The numerical model shows a fundamental change in the profile of the interfacial stress with a maximum stress concentration around the agglomeration and the interface. In the case of composites reinforced with rigid particles, the damage initiation occurs in these zones or near polymer/particle interfaces, where the stress is the highest due to the property mismatch [50]. Therefore, it is important to control the distribution of particles through the suspension in order to create a homogeneous distribution with minor aggregates and to obtain uniform mechanical properties.

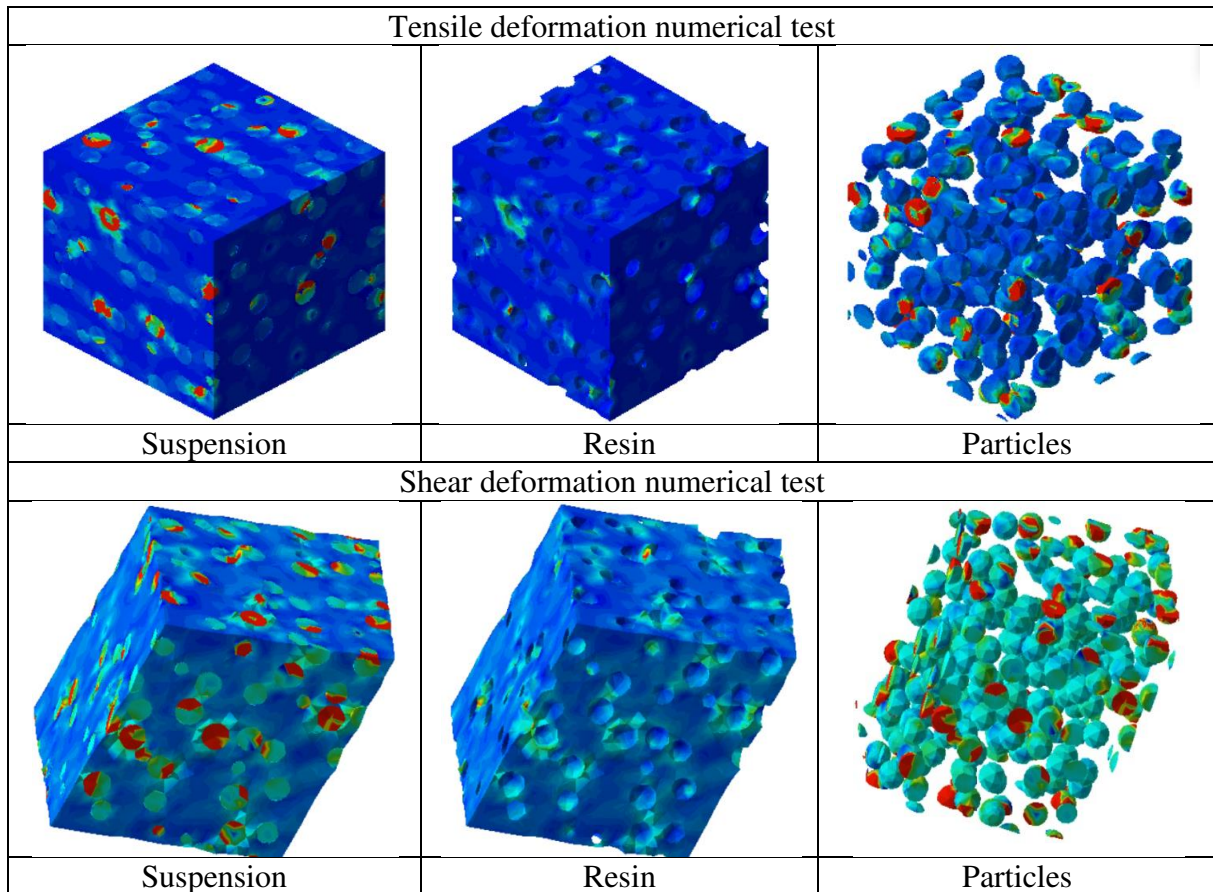


Figure 15: Stress concentration in the suspension reinforced with rigid particles under tensile and shear tests. The red color shows the maximum stress

4.4. Mechanical behavior of UD fibrous media reinforced with rigid spheres

In this section, we focus on the modeling of the mechanical behavior of the suspension and the composite in order to demonstrate the ability of the proposed approach to couple the process parameters and the composite mechanical properties. For the computation of the mechanical properties of the suspension, we recall that the epoxy resin and the alumina particles used in this study have Young's modulus of 5 GPa and 500 GPa, respectively.

The simulations presented hereafter aim at evidencing the importance of taking into account the effect of RTM process parameters on the mechanical properties of the composite. To do this, a numerical study was conducted to analyze the effect of the addition of particles in the composite and especially their distribution on the mechanical properties. The suspension was injected in the direction of the longitudinal fibers, as presented in Figure 16.

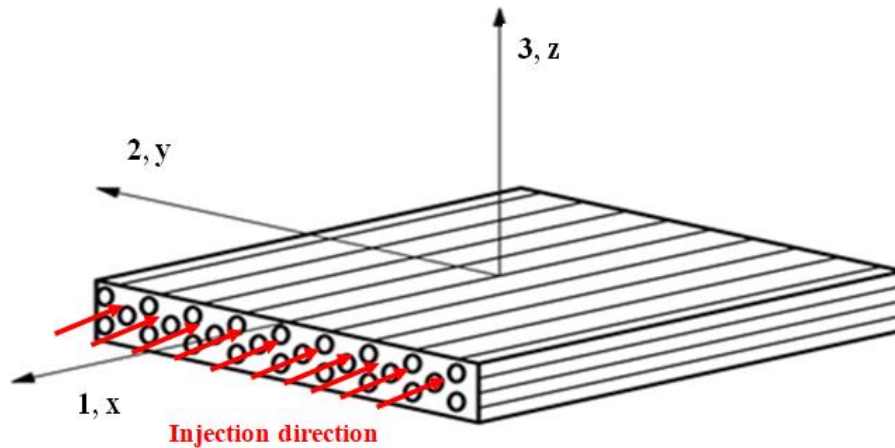


Figure 16: Injection strategy. The injection direction of the suspension is parallel to the longitudinal direction of UD fibers.

4.4.1. Mechanical behavior of the suspension

MT models, validated with experimental and numerical results, are used to determine the young's modulus E of the suspension. Figure 17 shows the spatial distribution of Young's modulus of the suspension in the fibrous medium at the end of injection, for different final injection times. The maximum value of Young's modulus of the suspension is obtained in the vicinity of the injection threshold, where the highest concentration of particles is observed (Figure7). This Young's modulus evolves according to a decreasing profile and a non-homogeneous distribution along with the fibrous medium. The Young's modulus value of the pure resin is 5GPa. At the end of the total impregnation of the preform ($t=58s$), a high concentration of particles, higher than 15%, has been distributed along the $\frac{3}{4}$ of the preform (Figure7), which leads to a clear improvement of Young's modulus of the suspension from 5GPa to 7.5 GPa, approximately. While in the zone located towards the end of the preform (not rich in particles), Young's modulus is close to 5.5 GPa.

The overflow resin and the total duration of the injection affect the mechanical properties of the suspension. For example, it appears that a clear amelioration is obtained in Young's modulus profile at time 70s ($E \geq 6.5GPa$), and a quasi-constant profile was obtained for 80, 90 and 100s ($E \geq 7.3GPa$). By increasing the total injection time, the suspension migrates to the particle poor zone and the polymer becomes more-particle rich in this zone and leading to an improvement of its mechanical properties.

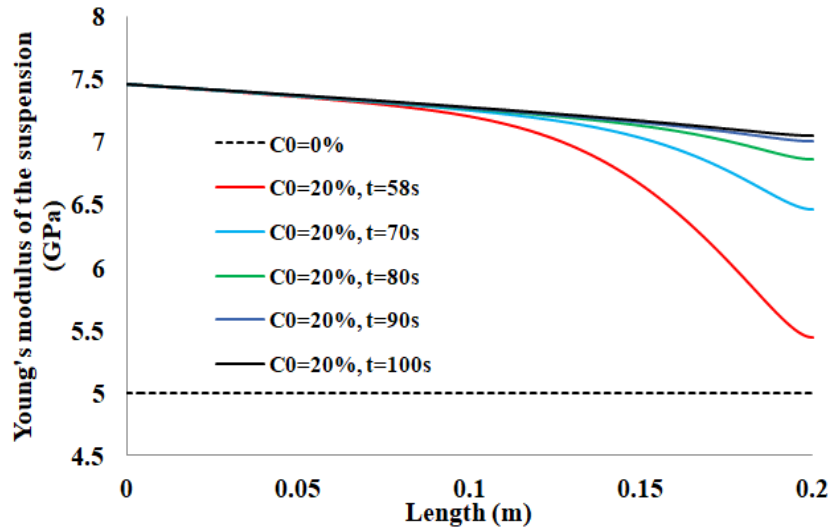


Figure 17: Spatial distribution of Young's modulus of the suspension in the fibrous media for different final injection times.

4.4.2. Mechanical behavior of the composite (UD fibers and the suspension)

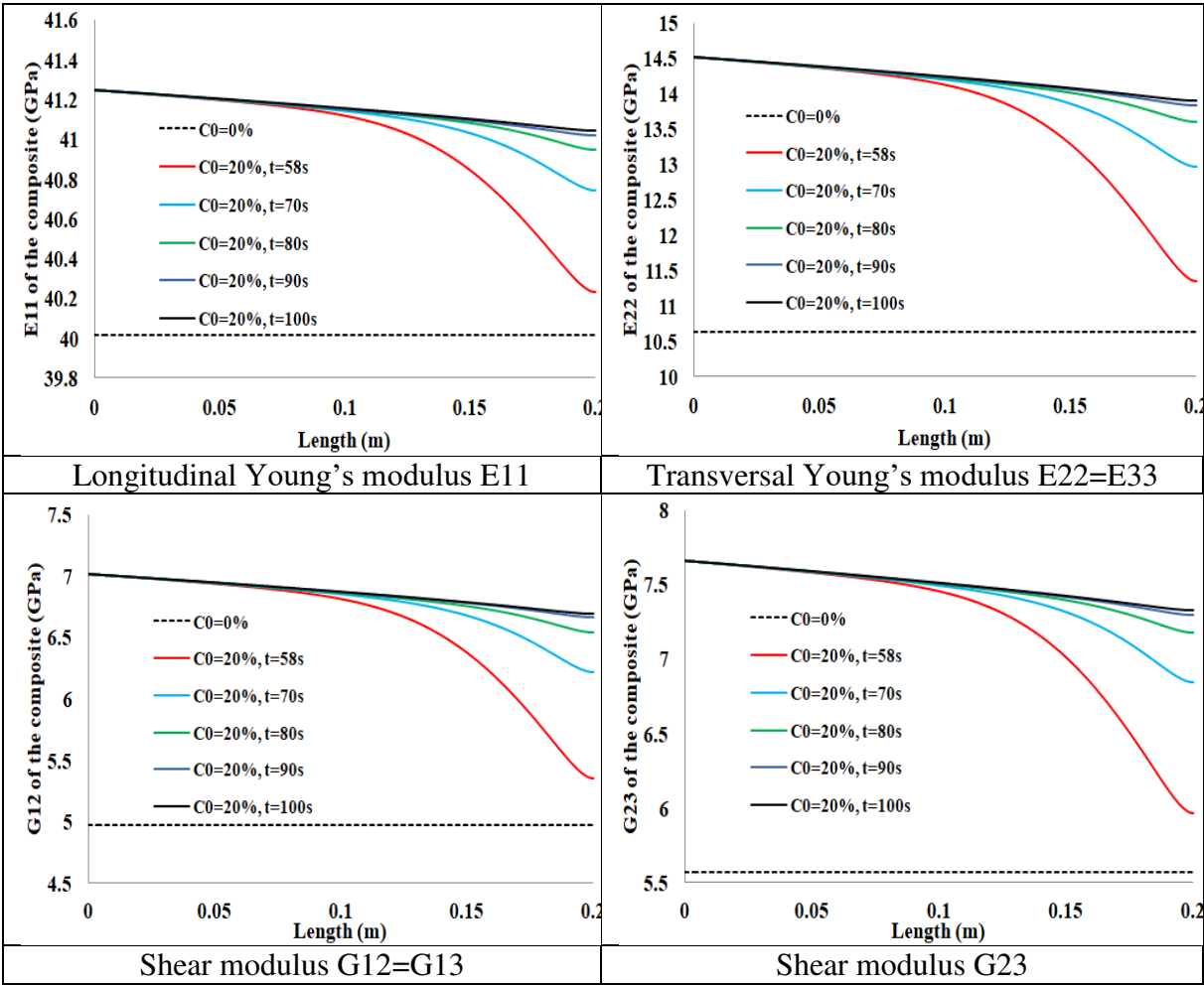
In this second step of the homogenization, we are interested in the prediction of the mechanical properties of the composite (UD + suspension), induced according to the different total injection duration. These properties of the composite will be identified using the epoxy Poisson ratio of 0.3 and Young's modulus of the suspension (calculated previously, see Figure 17), and those of the fibrous medium which are $E=75$ GPa for the Young's modulus and 0.2 for the Poisson ratio.

It should be noted that for the case of UD fibers reinforced with spherical particles, Hashin and Rosen model [51] is considered as the most used approach to estimate the mechanical properties of UD composites, namely the nine elastic moduli of the composite (three principal Young's moduli E_{11} , E_{22} , E_{33} , three principal shear moduli G_{12} , G_{13} , G_{23} and Poisson ratio ν_{12} , ν_{13} and ν_{23}). In the first instance, this model was initially validated in this study, with experimental data of Mbacke et al. [52] and the comparison was presented in Table 5. A good estimation of the mechanical properties was obtained using this model. Therefore, Hashin and Rosen model was subsequently used in this study.

	E_{11}	E_{22}	G_{12}	G_{23}	ν_{12}	ν_{23}
Experimental data [52]	45.0	12.0	4.5	-	0.3	-
Hashin and Rosen model [51]	45.11	12.24	4.06	4.26	0.26	-

Table 5: Mechanical properties of 60% UD glass fibers composites: validation of the analytical model with the experimental data.

The variation of the mechanical properties of glass fibers reinforced with the suspension is determined as a function of the process parameters and presented in Figure 18. From this figure, it appears that an important improvement of the transversal Young's modulus (E_{22} and E_{33}) and the shear moduli (G_{12} and G_{23}) was obtained compared with the case of $C_0=0\%$ (non-reinforcement). Results prove that the injection of particles through fibrous media leads to improvement of the out-of-plane mechanical properties (E_{33} and G_{23} associated with Z-direction) because the particle behavior is dominant compared with the X-direction where the glass fibers behavior is dominant.



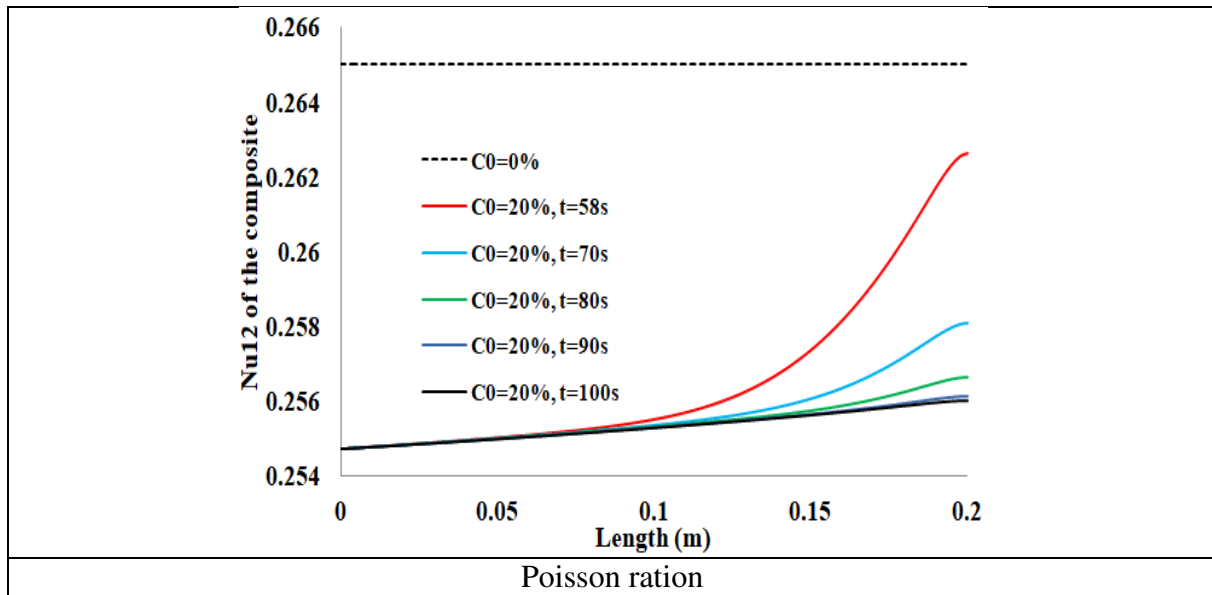


Figure18: Mechanical behavior of UD composites initially reinforced with 20% of rigid spheres for different total duration injections.

The evolution of mechanical properties of UD-composites was shown in Figure 18 for different total duration injections. For example, the transversal Young's moduli E22 and E33 of neat composites are 10.5 GPa, and with the injection of particle for t=58 s, these moduli become 14.5 GPa. If the filtration continues for several times [58s, 100s], the particles migrate to the other mold side (vent) which improves the mechanical properties of composites and keeps out air. A direct correlation between mechanical properties and injection time was observed. Therefore, a quasi-constant profile of mechanical properties was obtained for t=80, 90 and 100s. No important modification in terms of the Poisson ratio and E11 was observed by injecting the rigid particles through the UD fibers.

5. Conclusion

In this study, a complete model, which simulates the manufacturing of a particle-filled composite by RTM process and the prediction of its induced mechanical properties has been proposed. This global modeling approach combines (i) a numerical model which simulates the injection of particle-filled resins during the RTM process and (ii) computational homogenization methods of the mechanical properties of composites using the out-put results of (i)-step. In this approach, the main idea is to take into account the process influence on the induced mechanical properties of particle-filled composites. It has been formulated by a process/properties coupling and obtained by the simultaneous simulation of the process and the calculation of the mechanical properties induced by this process.

The numerical and analytical models proposed in this modeling approach have been compared and validated with experimental results. Some obtained results have then been presented to illustrate the capability of the proposed model. The pertinence of the proposed method is confirmed by predicting the nine elastic moduli of the composite (E11, E22, E33, G12, G13, G23, Nu12, Nu13, and Nu23) as a function of the particle concentration distribution obtained at the injection end. More importantly, to describe the evolution of these moduli as a function of the total injection duration. This last parameter proved to be crucial in the RTM process, as it allows to better control of the final particle distribution and consequently, to optimize the mechanical properties of the composite. The obtained results show that the injection of the rigid particle through UD fibers by RTM process improves the out-of-plane mechanical properties E22, E33, G12 and G23. For the case of the longitudinal Young's modulus E11, no important amelioration was observed.

- **Appendix A: constant for analytical model**

$$\begin{aligned}
A &= 8\left(\frac{G_i}{G_m} - 1\right)(4 - 5\nu_m)\eta_1 p^{\frac{10}{3}} - 2\left(63\left(\frac{G_i}{G_m} - 1\right)\eta_2 + 2\eta_1\eta_3\right)p^{\frac{7}{3}} + 252\left(\frac{G_i}{G_m} - 1\right)\eta_2 p^{\frac{5}{3}} \\
&\quad - 50\left(\frac{G_i}{G_m} - 1\right)(1 - 12\nu_m + 8\nu_m^2)\eta_2 p + 4(7 - 10\nu_m)\eta_2\eta_3 \\
B &= -4\left(\frac{G_i}{G_m} - 1\right)(1 - 5\nu_m)\eta_1 p^{\frac{10}{3}} + 4\left(63\left(\frac{G_i}{G_m} - 1\right)\eta_2 + 2\eta_1\eta_3\right)p^{\frac{7}{3}} - 504\left(\frac{G_i}{G_m} - 1\right)\eta_2 p^{\frac{5}{3}} \\
&\quad + 150\left(\frac{G_i}{G_m} - 1\right)(3 - \nu_m)\nu_m\eta_2 p + 3(15\nu_m - 7)\eta_2\eta_3 \\
C &= 4\left(\frac{G_i}{G_m} - 1\right)(5\nu_m - 7)\eta_1 p^{\frac{10}{3}} - 2\left(63\left(\frac{G_i}{G_m} - 1\right)\eta_2 + 2\eta_1\eta_3\right)p^{\frac{7}{3}} + 252\left(\frac{G_i}{G_m} - 1\right)(5\nu_m - 1)\eta_1 p^{\frac{10}{3}} \\
&\quad + 25\left(\frac{G_i}{G_m} - 1\right)(\nu_m^2 - 7)\eta_2 p - (7 + 5\nu_m)\eta_2\eta_3 \\
\eta_1 &= \left(\frac{G_i}{G_m} - 1\right)(49 - 50\nu_i\nu_m) + 35\frac{G_i}{G_m}(\nu_i - 2\nu_m) + 35(2\nu_i - \nu_m) \\
\eta_2 &= \frac{G_i}{G_m}(7 + 5\nu_i) + 4(7 - 10\nu_i) \\
\eta_3 &= \frac{G_i}{G_m}(8 - 10\nu_m) + 7 - 5\nu_m
\end{aligned}$$

Declaration

Funding

The authors declare that no funds, grants, or other support were received during the preparation of this manuscript.

Conflict of interest/ Competing Interests

The authors declare no competing interests/ The authors have no relevant financial or non-financial interests to disclose.

Code availability

Not applicable.

Availability of data and materials

The authors declare that the data and the materials of this study are available within the article.

Ethical approval

All procedures performed in studies involving human participants were in accordance with the ethical standards of the institutional and/or national research committee and with the 1964 Helsinki declaration and its later amendments or comparable ethical standards.

Consent to participate

Informed consent was obtained from all individual participants included in the study.

Consent to publish

The participants have consented to the submission of the case report to the journal.

Authors' contributions

A. El Moumen and A. Saouab: construct the idea. A. El Moumen: developed numerical model and performed numerical simulation, analyzed data, draft manuscript preparation, and wrote the paper. A. Saouab: analyzed results, analyzed numerical model, and co-wrote the paper. A. Imad and T. Kanit discuss the results, correct the English and the paper format. All authors reviewed the results, prepared the response to reviewer comments, and approved the final version of the manuscript.

References

- [1] Djebara Y, Imad A, Saouab A, Kanit T. A numerical modelling for resin transfer molding (RTM) process and effective thermal conductivity prediction of a particle-filled composite carbon-epoxy. *J Compos Mater* (2020); 55:3–15.
- [2] Chohra M, Advani SG, Yariagadda S. Filtration of particles through a single layer of dual scale porous media. *Adv Compos Lett* (2007) 16:205–221
- [3] Steggall-Murphy C, Simacek P, Advani SG, Yariagadda S, Walsh S. A model for thermoplastic melt impregnation of fiber bundles during consolidation of powder-impregnated continuous fiber composites. *Composites Part A* (2010) 41:93–100
- [4] Nordlund M, Fernberg SP, Lundström TS. Particle deposition mechanisms during processing of advanced composite materials. *Compos Part A* (2007) 38:2182–2193
- [5] Tarfaoui M, El Moumen A, Boehle M, Shah O, Lafdi K. Self-heating and deicing epoxy/glass fiber based carbon nanotubes buckypaper composite. *J Mater Sci* (2019) 54:1351–1362
- [6] Shaker K, Nawab Y, Saouab A. Influence of silica fillers on failure modes of glass/vinyl ester composites under different mechanical loadings. *EngFract Mech* (2019) 218:106605.
- [7] Shaker K, Nawab Y, Saouab A. Experimental and numerical investigation of reduction in shape distortion for angled composite parts. *Int J Mater Form* (2019) 11. <https://doi.org/10.1007/s12289-019-01510-6>
- [8] Xie F, Pollet E, Halley PJ, Avérous L. Starch-based nano-biocomposites. *Prog Polym Sci* (2013) 38:1590–1628

- [9] Manfredi E, Michaud V. Packing and permeability properties of E-glass fibre reinforcements functionalised with capsules for self-healing applications. *Compos. Part A Appl. Sci. Manuf.* (2014) 66: 94-102.
- [10] Louis BM, Maldonado J, Klunker F, Ermanni P. Particle distribution from in-plane resin flow in a resin transfer molding process. *Polym. Eng. Sci.* (2019) 59: 22-34.
- [11] Sandler JKW, Kirk JE, Kinloch IA, Shaffer MSP, Windle AH. Ultra-Low Electrical Percolation Threshold in Carbon-Nanotube-Epoxy Composites. *Polymer (Guildf)*. (2003) 44: 5893–5899
- [12] Andrianov IV, Danishevs'Kyy VV, Kalamkarov AL. Analysis of the effective conductivity of composite materials in the entire range of volume fractions of inclusions up to the percolation threshold. *Compos. Part B Eng.* (2010) 41: 503-507.
- [13] Lee GW, Park M, Kim J, Lee JI, Yoon HG. Enhanced thermal conductivity of polymer composites filled with hybrid filler. *Compos. Part A Appl. Sci. Manuf.* (2006) 37: 727-734.
- [14] Qian L, Pang X, Zhou J, Yang J, Lin S, Hui D. Theoretical model and finite element simulation on the effective thermal conductivity of particulate composite materials. *Compos. Part B Eng.* (2017) 116 : 291-297.
- [15] Guan FL, Gui CX, Zhang HB, Jiang ZG, Jiang Y, Yu ZZ. Enhanced thermal conductivity and satisfactory flame retardancy of epoxy/alumina composites by combination with graphene nanoplatelets and magnesium hydroxide. *Compos. Part B Eng.* (2016) 98: 134-140.
- [16] Fernberg SP, Sandlund EJ, Lundström T. Mechanisms Controlling Particle Distribution in Infusion Molded Composites. *Journal of Reinforced Plastics and Composites.* (2006) 25: 59-70.
- [17] Wang YH, et al. Activated carbon spheres@NiCo₂(CO₃)_{1.5}(OH)₃ hybrid material modified by ionic liquids and its effects on flame retardant and mechanical properties of PVC. *Compos. Part B Eng.* (2019) 179: 107543.
- [18] Kashiwagi T, Du F, Douglas JF, Winey KI, Harris RH, Shields JR. Nanoparticle networks reduce the flammability of polymer nanocomposites. *Nat. Mater.* (2005) 4: 928-933.
- [19] Mirzaei AH, Shokrieh MM. Simulation and measurement of the self-heating phenomenon of carbon/epoxy laminated composites under fatigue loading. *Composites Part B: Engineering* (2021) 223: 109097
- [20] Benyahia H, Tarfaoui M, Datsyuk V, El Moumen A, Trotsenko S, Reich S. Dynamic properties of hybrid composite structures based multiwalled carbon nanotubes. *Composites Science and Technology* (2017) 148: 70-79.
- [21] Tarfaoui M, El Moumen A, Lafdi K, Hassoon OH, Nachtane M. Inter laminar failure behavior in laminate carbon nanotubes-based polymer composites. *Journal of Composite Materials* (2018) 52: 3655-3667.
- [22] Tagliavia G, Porfiri M, Gupta N. Analysis of flexural properties of hollow-particle filled composites. *Compos. Part B Eng.* (2010) 41: 86-93.
- [23] Zhang X, et al. The effect of strain rate and filler volume fraction on the mechanical properties of hollow glass microsphere modified polymer. *Compos. Part B Eng.* (2016) 101: 5363.
- [24] Porfiri M, Gupta N. Effect of volume fraction and wall thickness on the elastic properties of hollow particle filled composites. *Compos. Part B Eng.* (2009) 40: 166-173.
- [25] Lefevre D, Comas-Cardona S, Binétry C, Krawczak P. Modelling the flow of particle-filled resin through a fibrous preform in liquid composite molding technologies. *Compos. Part A Appl. Sci. Manuf.* (2007) 38: 2154-2163.
- [26] Haji H, Saouab A, Nawab Y. Simulation of coupling filtration and flow in a dual scale fibrous media. *Compos. Part A Appl. Sci. Manuf.* (2015) 76: 272-280.
- [27] Nordlund M, Fernberg SP, Lundström ST. Particle deposition mechanisms during processing of advanced composite materials. *Compos. Part A Appl. Sci. Manuf.* (2007) 38: 2182-2193.
- [28] Sas HS, Erdal M. Modeling of particle–resin suspension impregnation in compression resin transfer molding of particle-filled, continuous fiber reinforced composites. *Heat Mass Transfer* (2014) 50: 397-414.
- [29] Erdal M, Guceri SI, Danforth SC. Impregnation molding of Particle-Filled preceramic polymers: process modeling. *J Am Ceram Soc* (1999) 82: 2017–2028

- [30] Lefevre D, Comas-Cardona S, Binetruy C, Krawczak P. Coupling filtration and flow during liquid composite molding: Experimental investigation and simulation. *Compos Sci Technol* (2009) 69: 2127–2134.
- [31] Qian E, Huang N, Lu J, Han Y. CFD–DEM simulation of the filtration performance for fibrous media based on the mimic structure. *Computers and Chemical Engineering* (2014) 71: 478–488.
- [32] Abliz D, Berg DC, Ziegmann G. Flow of quasi-spherical nanoparticles in liquid composite molding processes. Part II: Modeling and simulation. *Composites Part A* (2019) 125: 105562.
- [33] Reia da Costa EF, Skordos AA. Modelling flow and filtration in liquid composite moulding of nanoparticle loaded thermosets, *Composites Sciences and Technology* (2012) 72: 799-805.
- [34] El Moumen A, Saouab A, Siddig NA, Bizet L, Imad A. Numerical study to control the filler distribution in fibrous media during the particle-filled resin transfer molding process. *Int J Adv Manuf Technol* (2021) 114: 1669.
- [35] Haji H, Saouab A, Park C H. Particles Deposit Formation and Filtering: Numerical Simulation in the Suspension Flow Through a Dual Scale Fibrous Media. *Macromolecular Symposia Volume* (2014) 340: 44-51.
- [36] Kang S, Lee H, Kim S, Chen D, Pui D. Modeling of fibrous filter media for ultrafine particle filtration. *Separation and Purification Technology* (2019) 209: 461-469.
- [37] El Moumen A, Kanit T, Imad A. Numerical evaluation of the representative volume element for random composites. *European Journal of Mechanics - A/Solids* (2021) 86: 104181
- [38] Sukiman MH, Kanit T, N'Guyen F, Imad A, El Moumen A, Erchiqui F. Effective thermal and mechanical properties of randomly oriented short and long fiber composites. *Mechanics of Materials* (2017) 107 : 56-70.
- [39] El Moumen A, Tarfaoui M, Lafdi K. Computational Homogenization of Mechanical Properties for Laminate Composites Reinforced with Thin Film Made of Carbon Nanotubes. *Applied Composite Materials volume* (2018) 25: 569–588.
- [40] El Moumen A, N'Guyen F, Kanit T, Imad A. Mechanical properties of poly–propylene reinforced with Argan nut shell aggregates: Computational strategy based microstructures. *Mechanics of Materials* (2020) 145: 103348.
- [41] Rintoul MD, Torquato S. Reconstruction of the structure of dispersions, *Journal of Colloid and Interface Science* (1997) 186: 467–476.
- [42] Segurado J, Llorca J. A numerical approximation to the elastic properties of sphere-reinforced composites, *Journal of the Mechanics and Physics of Solids* (2002) 50: 2107–2121.
- [43] El Moumen A, Kanit T, Imad A, El Minor H. Effect of reinforcement shape on physical properties and representative volume element of particles-reinforced composites: statistical and numerical approaches. *Mechanics of Materials* (2015) 83: 1-16.
- [44] El Moumen A, Kanit T, Imad A, El Minor H. Computational thermal conductivity in porous materials using homogenization techniques: numerical and statistical approaches. *Computational Materials Science* (2015) 97: 148-158.
- [45] Al Habis N, El Moumen N, Tarfaoui M, Lafdi K. Mechanical properties of carbon black/poly(e-caprolactone)-based tissue scaffolds. *Arabian Journal of Chemistry* (2020) 13: 3210-3217.
- [46] Mori T, Tanaka K. Average stress in matrix and average elastic energy of materials with misfitting inclusions. *Acta Metall.* (1973) 21: 571-574.
- [47] Hashin Z, Shtrikman S. A variational approach to the theory of the elastic behaviour of multiphase materials. *J. Mech. Phys. Solids* (1963) 11: 127-140.
- [48] Christensen RM, Lo KH. Solutions for effective shear properties in three phase sphere and cylinder models. *J. Mech. Phys. Solids* (1979) 27: 315-330.
- [49] Al-Namie I, Ibrahim A, Hassan MF. Study the Mechanical Properties of Epoxy Resin Reinforced With silica (quartz) and Alumina Particles. *The Iraqi Journal For Mechanical And Material Engineering* (2011) 11: 486-506.
- [50] Saoudi T, El Moumen A, Kanit T, Belouchrani MA, Benseddiq N, Imad A. Numerical Evaluation of the Thermal Properties of UD-Fibers Reinforced Composites for Different Morphologies. *International Journal of Applied Mechanics* (2020) 12: 2050032.
- [51] Hashin Z, Rosen W. The elastic moduli of fiber reinforced materials. *Journal of applied mechanics* (1964) 31: 223–232.

[52] M. Mbacke. Characterization and modeling of mechanical behavior of 3D braided composites: Application to design of NGV tanks. (2014) HAL Id: pastel-00960667. <https://pastel.archives-ouvertes.fr/pastel-00960667>